High Temperature Sodium Submersible Flowmeter Design and Analysis

Matthew Weathered, Christopher Grandy, Mark Anderson, Darius Lisowski

***Abstract*—This work details the design and analysis of a permanent magnet flowmeter designed to be submerged in a pool type sodium fast reactor environment. Recently developed Samarium Cobalt rare earth magnets were utilized that have demonstrated resilience to temperature and neutron flux up to 550 °C and 10^{18} n/cm^2, respectively. This paper will discuss the theory, design, calibration and uncertainty quantification of the flowmeter. The flowmeter was calibrated over a flowrate range of 11.4 - 90.9 LPM at temperatures of 220 and 400 °C, yielding an uncertainty in calibration of 2-3.6%. A finite element model was developed and validated experimentally, yielding <3.2% error.**

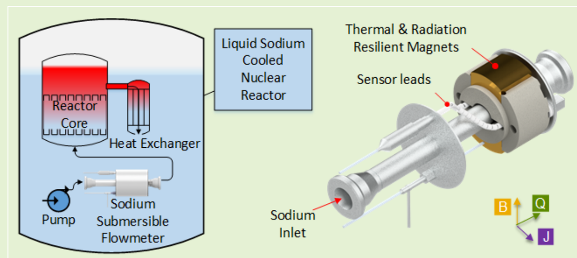

***Index Terms*—Calibration, Fluid flow measurement, Lithium, Nuclear power generation, Potassium, Sodium**

Nomenclature

B	Magnetic field flux density
B_r	Remanent flux density
B_R	Bias limit
C	Calibration coefficient
$\bar{C}$	Average calibration coefficient
C_i	Calibration coefficient of ith measurement
D	Outer diameter, flow tube
d	Inner diameter, flow tube
E	Electric field
F	Lorentz force
J	Current density
K_B	K-factor, magnetic field
K_E	K-factor, end shunting
K_W	K-factor, wall shunting
L	Axial length of magnets
N	Number of measurements
Q	Flowrate
Q_{IUT}	Flowrate, instrument under test
Q_{REF}	Flowrate, reference instrument
S_R	Precision index
T_m	Temperature, magnet
T_s	Temperature, sodium
$U_{C,\sigma}$	Type A uncertainty
v	Fluid velocity
V_m	Measured voltage
δ	Hartman layer thickness
ϵ_r	Permittivity
μ_0	Permeability constant
μ_r	Relative permeability
μ_v	Dynamic viscosity
ρ_e	Electrical resistivity
σ	Standard deviation
σ_e	Electrical conductivity

Support for this work was provided by the Department of Energy's Office of Nuclear Energy Advanced Reactor Technologies Program and funding through the Nuclear Energy University Program DE-FOA-0001913.

M. Weathered is a Research Scientist at Argonne National Laboratory, Lemont, IL 60439 USA (e-mail: mweathered@anl.gov).

C. Grandy is a Program Manager at Argonne National Laboratory, Lemont, IL 60439 USA (e-mail: cgrandy@anl.gov).

M. Anderson is a Professor at the University of Wisconsin-Madison, Madison, WI 53706 USA (e-mail: manderson@engr.wisc.edu).

D. Lisowski is a Group Manager at Argonne National Laboratory, Lemont, IL 60439 USA (e-mail: dlisowski@anl.gov).

I. Introduction

LIQUID sodium is a prime candidate for Generation-IV nuclear reactor coolants given its high boiling, excellent thermal conductivity, and favorable neutronic properties. In a pool type sodium cooled reactor, the core and the primary heat transport system are installed in a single vessel; this design provides radiation confinement and a large thermal mass around the core to reduce the likelihood of a complete loss of heat sink in the reactor. Unfortunately, this design poses a challenge when attempting to measure key coolant parameters near the core such as flow rate, as you must engineer a system to be submerged in a high temperature, high radiation, molten metal environment.

A comprehensive overview of liquid metal flow measurement can be found in [1] as well as [2]. The high reliability, good linearity, large flow range, low pressure drop, and near instant response time make the permanent magnet flow meter an attractive device for sodium flow rate measurement. However, magnet technology of the past limited the use of these flow meters.

The performance of a permanent magnet can be quantified by the maximum energy product. ALNICO magnets, composed primarily of aluminum, nickel, and cobalt, have been used historically in permanent magnet flow meters for high temperature liquid sodium, allowing maximum operating temperatures near 550 °C. However, the maximum energy product of the ALNICO magnets, on the order of 43.8 kJm^{-3} for ALNICO 5, is typically lower than rare earth magnets, such as neodymium and samarium cobalt, at around 256 and 192 kJm^{-3}, respectively [3]. A lower maximum energy product means an ALNICO flowmeter is relatively bulky as the magnets must be large to produce a reasonable signal to noise ratio in the meter. This low energy product is due to the ALNICO magnet's low coercivity, or resistance to demagnetization [4]. In the past, rare earth magnets have been limited to a maximum operating temperature of 80 and 350 °C for neodymium and samarium cobalt, respectively. Recently, samarium-cobalt magnets with a maximum operating temperature of 550 °C and radiation resilience of $\geq 10^{18}\ n/cm^2$ have become commercially available [5].

In this work an Argonne National Laboratory designed electromagnetic submersible flow meter (ANL EMFM) was built using cutting edge rare earth magnets that can be submerged in a sodium cooled reactor environment. This paper begins with an overview of flow meter theory, introducing a semi-empirical equation that can be used to translate induced voltage into a measured flow rate. Next, the design of the flowmeter will be discussed. A finite element analysis will be introduced that was validated with experimental data. Finally a description of the flow meter calibration and subsequent uncertainty analysis will be provided.

Ultimately, this flow meter will be installed in the Mechanisms Engineering Test Loop (METL) to characterize under sodium flow rate in the Thermal Hydraulic Experimental Test Article (THETA) [6], [7].

II. Flow Meter Theory

A permanent magnet flow meter utilizes a permanent magnetic field positioned perpendicularly to a flow of electrically conductive fluid to induce a transverse voltage across the flow. The fundamental physics that drive the electric and magnetic field development in the flowmeter via a Lorentz force are captured by Ohm's law, (1) [8].

$$J = \sigma_e(E + v \times B) \tag{1}$$

When sodium with electrical conductivity of σ_e flows at velocity v through a magnetic field B set up by the permanent magnets, the relative motion yields a proportional electric current J and an electric field E is generated by the combination of the magnetic field and the current.

This induced electric potential can be measured with leads welded onto the flow tube at diametrically opposed positions; the volumetric flow rate can be calculated as a function of this induced voltage with the semi-empirical (2) [9], [10].

$$Q = C\ Q_{IUT} = C\frac{\pi V_m d}{4BK_BK_WK_E} \tag{2}$$

Where Q_{IUT} is the un-calibrated flow rate of the instrument under test, C is a linear calibration coefficient, V_m is the measured voltage, d is the internal diameter of the flow tube, and B is the flowmeter magnetic flux density. K_B is a coefficient that accounts for the reduction in magnetic field strength at high temperatures, (3). K_W is a coefficient that accounts for a shunting effect whereby the generated current bypasses the sodium through the flow tube wall, (4). K_E accounts for a shunting effect that occurs when charge recombination occurs at the entrance and exit of the flowmeter where the magnetic field is the weakest, (5).

$$K_B = \frac{(-7E-07)T_m^2 - (2E-04)T_m + .8587}{0.8587} \tag{3}$$

$$K_W = \frac{2d/D}{(1+(\frac{d}{D})^2) + \rho_{e,ratio}(1-(\frac{d}{D})^2)} \tag{4}$$

$$\begin{aligned} K_E = -0.0047(\frac{L}{d})^4 + 0.0647(\frac{L}{d})^3 - 0.3342(\frac{L}{d})^2 + \\ 0.7729(\frac{L}{d}) + 0.3172 \end{aligned} \tag{5}$$

Where T_m is the magnet temperature in degrees Celsius, L is the length of the flowmeter encompassed by the physical permanent magnets and ρ_{sodium} is the electrical resistivity of sodium [11] and ρ_{ss316} is the electrical resistivity of the 316 stainless steel tube material [12]. Equation (6) provides a second order polynomial for the ratio of resistivities [10].

$$\begin{aligned} \rho_{e,ratio} = \frac{\rho_{e,sodium}}{\rho_{e,ss316}} = (1.3988E-07)T_s^2 + \\ (2.4551E-04)T_s + (8.2632E-02) \end{aligned} \tag{6}$$

Note that (3) was calculated by fitting a second order polynomial with R^2=0.9997 to the data for remanence as a function of temperature for EEC 18-T550 magnets, provided by the manufacturer in Fig. 1.

The calibration coefficient C in (2) would ideally be one if the above semi-empirical K factors accounted for all of the subtle pheneomena in the flowmeter. However, as will be seen in Section V the calibration coefficient is typically non-unity and is not necessarily independent of flow rate.

III. Flowmeter Design

As can be seen in Fig. 2, all exposed surfaces of the flow meter are 316 stainless steel, an alloy with excellent material compatibility with liquid sodium [14]. This allows the flow meter to be submerged completely in sodium where determination of in-pool flow rates is required. The flow meter has a maximum allowable external working pressure of 1,045 kPa at a temperature of 550 °C, calculated according to Figures G and HA-2 in ASME BPVC Section II, Part D 2019.

Samarium cobalt magnets were sourced for this flow meter as they possess a higher coercivity and energy product than the ALNICO-5 magnets used in past permanent magnet based submersible flow meters [15]. This means the flow meter size and weight may be reduced while maintaining the same induced voltage flow signal.

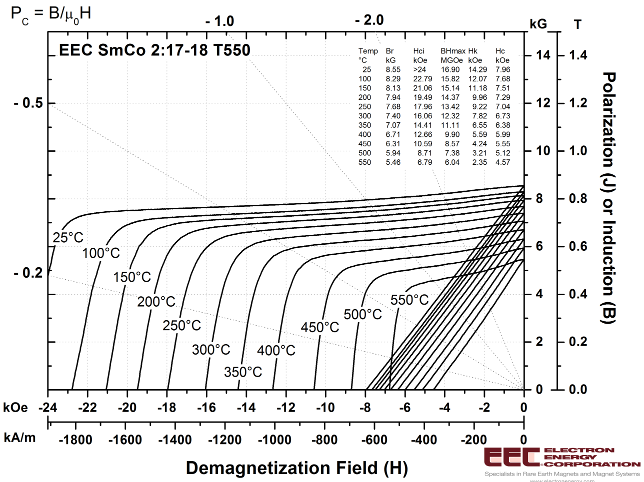

Fig. 1. Induction vs Demagnetization of EEC 18-T550 Samarium Cobalt magnets. Provided here with express written permission from manufacturer, Electron Energy Corporation [13]

The magnets used were custom machined samarium cobalt (Sm_2Co_{17}) T550 ultra high temperature magnets from Electron Energy Corporation, (mfg. PN: EEC 18-T550). A 17.8 μm electroless coating of nickel was plated onto the magnets after machining to enhance the high temperature corrosion resistance of the magnets; in tests with similar magnets it was shown that a nickel coating of this approximate thickness would provide an improved magnetic field stability, as compared to an un-coated magnet, of 861% and 143% when exposed to temperatures of 500 °C in air and vacuum, respectively, for a period of 3,000 hrs [16].

The magnets were mounted to a 1018 steel yoke, positioning the magnets concentric with the flow tube and providing a preferential path for the magnetic field lines to improve the magnetic flux at the tube center, Fig. 3. Diametrically opposed 316 stainless steel wires were affixed to the flow tube at the center of the magnetic assembly using a high temperature braze (Silvaloy 721). While this introduces a dissimilar metal, effectively creating a thermocouple in the circuit, the signal wires were connected in an identical manner so their Seebeck voltages cancel out, as confirmed during calibration in Section V. In the future these sensor wires shall be welded to the flow tube with an identical filler material to eliminate the potential for this effect.

Stainless steel 316 sheathed cables with ceramic MgO insulation transmit measured voltage and temperature readings from the flow meter body, through the molten sodium, to the top of the pressure vessel. The voltage sensor wires in the cable were made of 310 stainless steel, while the thermocouple was a type-K.

The magnetic flux density was measured in the as-built flow meter at the tube center, in the center of the magnetic field, perpendicular to the permanent magnets. A measurement of 252 ± 0.1 mT was found with an F.W. Bell 5180 Gaussmeter at room temperature. This magnetic flux density will provide the B value when calculating the flow rate using (2).

IV. Finite Element Analysis

Finite element analysis (FEA) software may be used to predict the performance of the flow meter and validate the semi-empirical model of (2). When solving this magnetohydrodynamics (MHD) problem, one must couple the physics between the fluid, electric and magnetic phenomena by solving their respective partial differential equations. This analysis was performed by solving these differential equations simultaneously over a mesh of discrete elements using COMSOL Multiphysics V5.5.

The simulation geometry can be found in Fig. 4. As can be seen, there are 6 total domains: 1: sodium, 2: circular flow tube, 3: magnetic yoke, 4-5: two permanent magnets, and 6: air. The model was meshed using 208,919 elements with an average quality (skewness) of 0.656. The Hartmann layer, (7), is a boundary layer present on the periphery of a conductive fluid where the magnetic field is not tangential to the boundary [17], [18], [19]. In order to fully capture the MHD phenomena in domain 1 you must ensure the finite elements (mesh) near the boundary of the flow tube are similar in size to the Hartman layer thickness, in this case, approximately 30 μm.

$$\delta = \frac{\sqrt{\mu_v \rho_e}}{B} \tag{7}$$

In domain 1, the velocity field is affected by the electromagnetic field and must be accounted for to fully couple the solution by including a Lorentz force term to the flow, (8).

$$F = \begin{bmatrix} J_y B_z - J_z B_y \\ J_z B_x - J_x B_z \\ J_x B_y - J_y B_x \end{bmatrix} \begin{bmatrix} x & y & z \end{bmatrix} \tag{8}$$

In order to resolve the flow field in domain 1, the Reynolds-averaged Navier-Stokes (RANS) equations with the two equation K-epsilon turbulence model were solved [20].

In domain 1, Ohm's law was solved, (1) and in domain 1-2 Ampere's Law and current conservation equations were solved, (9)-(10).

$$\nabla \times \frac{B + B_r}{\mu_0 \mu_r} = J \tag{9}$$

$$\nabla \cdot J = 0 \tag{10}$$

In domains 3-6 there is no current flow so only (9) is solved for, where the current density is set to zero. The remanent flux density, B_r, is only nonzero in domains 4-5. In domain 1, a fully developed flow inlet boundary condition and zero gauge pressure outlet condition was applied, as well as a no slip boundary condition on the flow tube walls. In domain 6, a magnetic insulation boundary condition was applied to the outer boundary.

A summary of the pertinent material properties can be found in Table I for the FEA model at 400 °C. Note that the value for the permeability of a paramagnetic material such as 1018 steel, which forms the yoke of the flow meter magnets, is dependent on the magnetic field strength and shape. The relative permeability of 1018 steel can vary from about 5-100, depending on the applied external field [21]. An optimization

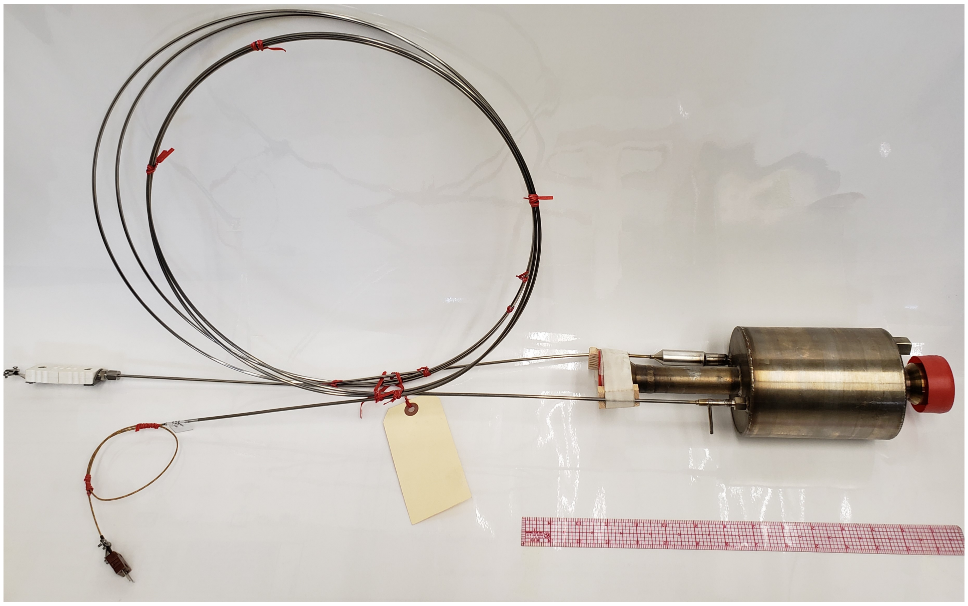

Fig. 2. Photograph of the ANL EMFM. The outer shell of the flow meter is a 10.2 cm (4”) diameter tube. The 2.4 m (8’) long signal wire and thermocouple feedthrough cables are coiled in this picture- they may be fed through 0.32 cm (0.125”) feedthrough holes in an enclosed experiment by removing the end connectors

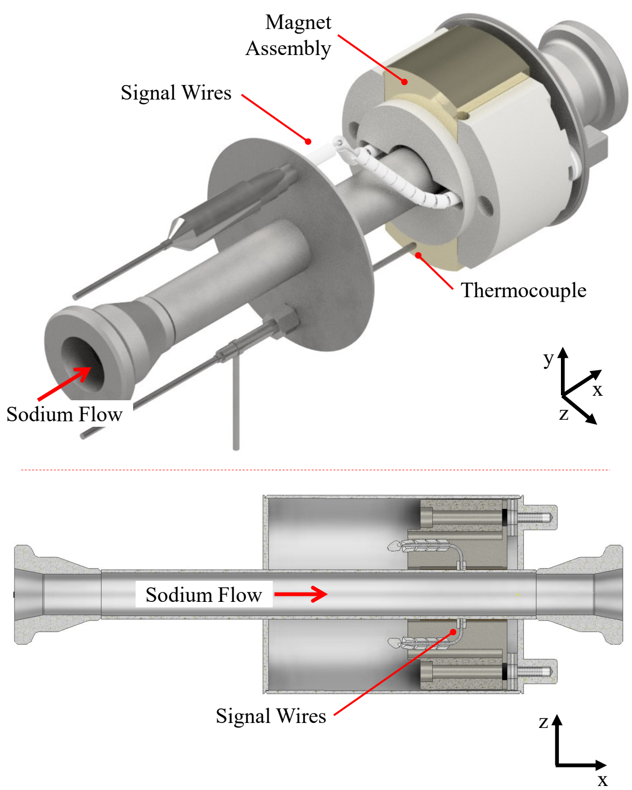

Fig. 3. Schematic of the ANL EMFM, isometric view showing flowmeter without housing (top), cross section view showing signal wires affixed to flow tube (bottom).

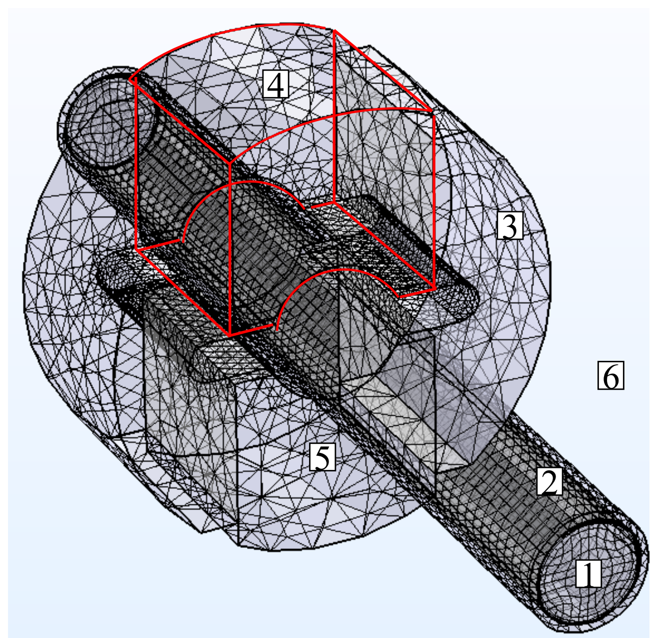

Fig. 4. Finite element analysis model showing mesh and 6 domains, 1: sodium, 2: circular flow tube, 3: magnetic yoke, 4-5: two permanent magnets, and 6: air domain

study was performed using an FEA model of the flow meter in air at room temperature- varying the relative permeability until the FEA magnetic flux density at the magnet assembly center matched the measured value of 252 mT in air at room temperature. A relative permeability of 60 produced a measured flux density of 252 mT. To give an idea of sensitivity, relative permeabilities of 5 and 100 produced a measured flux density of 286 and 247 mT, respectively.

Fig. 5 presents the velocity in the x direction as well as

TABLE I
FEA MATERIAL PROPERTIES

	Sodium	1018 Steel	316 SS	Air	Sm_2Co_{17}
ρ_e [10^{-8} Ω-m]	22.08	-	101.7	-	-
μ_r [-]	1.00	60	1.01	1.00	1.00
ϵ_r [-]	1.00	1.00	1.00	1.00	1.00
ρ [kg/m^3]	857.77	-	-	-	-
μ_v [Pa-s]	2.77E-04	-	-	-	-

Material properties at 400 °C. Electrical resistivity (ρ_e), relative permeability (μ_r), permittivity (ϵ_r), density (ρ) and dynamic viscosity (μ_v). [11], [12], [22], [23]

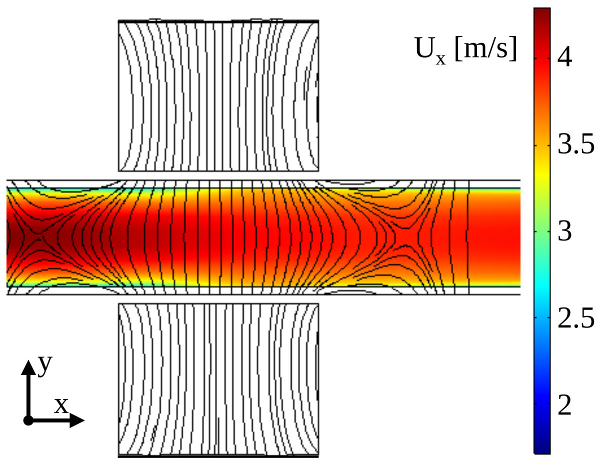

Fig. 5. Velocity in the x direction, $\boldsymbol{U_x}$, with black streamlines showing magnetic flux density through the cross section of the flow tube and permanent magnets. $\boldsymbol{T_m}$ and $\boldsymbol{T_s}$ at 400 °C, $\boldsymbol{Q}$=83.3 LPM (22 GPM).

streamlines showing magnetic flux density for 400 °C sodium flowing at 83.3 LPM. As can be seen, as the sodium encounters the upstream edge of the magnetic field, the end-currents begin to alter the fully developed flow profile. As the sodium then moves through the magnetic field, the velocity distribution begins to flatten out and turbulent kinetic energy is suppressed as a result of the jxB Lorentz force.

Fig. 6 presents the voltage measurement at locations that are at up and downstream axial locations as well as circumferential locations with respect to an ideal sensor lead that is perfectly positioned on the flow tube in the middle of both magnets and diametric to the second lead. This provides a measure of the sensitivity of the measured voltage to the as built location of the sensor lead. Ideally the sensor lead would be welded in the center of the axial and circumferential locations at x=0. As can be seen, the voltage output is more sensitive to the accuracy of the circumferential location. Using equations fitted to the FEA result in Fig. 6, one may calculate the voltage differential at a combined $\pm$ 1 mm axial and circumferential deviation relative to zero to be 13.1 μV, a 0.2% reduction in signal. Thus, as long as the location of the measurement leads are reasonably toleranced from a machining and welding standpoint, the sensitivity of the voltage to the axial and circumferential lead location is limited. This uncertainty contribution has been included in the flowrate error propagation for measured voltage, V_m, Table II.

A comparison between FEA and experimental results for induced voltage as a function of flow rate can be found in

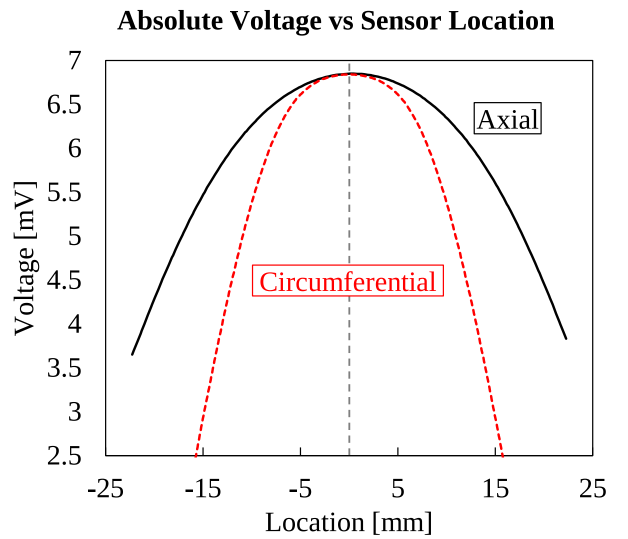

Fig. 6. Sensitivity study from the FEA analysis at 400 °C, 83.3 LPM showing the absolute measured voltage along the axial and circumferential location with respect to a theoretical sensor lead welded perpendicular to and in the center of the magnetic field. Axial trend line: $\boldsymbol{y = -0.0063x^2 + 0.0043x + 6.8989}$, Circumferential trend line: $\boldsymbol{y = 7E - 08x^6 - 6E - 08x^5 - 4E - 05x^4 + 2E - 05x^3 - 0.0116x^2 - 0.0013x + 6.8933}$, $\boldsymbol{R^2 = 0.999}$ for both trend lines.

Fig. 7. As can be seen, the FEA is validated with good correlation at temperatures of 220 and 400°C and flow rates of 11.4, 45.4, and 83.3 LPM. A maximum error for the FEA result with respect to experimental data of 3.2% was found.

The magnetohydrodynamic properties of the system are a non-linear function of temperature. Indeed, it can be difficult to utilize a semi empirical model, (2), with K factors derived from flow meter geometry of historical experiments, to predict induced voltages for all possible process conditions. Therefore, the FEA model developed herein can be utilized as a digital twin whereby a user can run realtime simulations of the flowmeter, inputting the actual system temperature and measured voltage to back out the system flowrate. A parametric sweep may be performed at all possible operating temperatures and flowrates to produce lookup tables for more efficient flow rate determination. This process may forgo an expensive flowmeter calibration. However in a critical application- a calibration is prudent to ensure quality of measurement, this will be detailed in the next section.

V. FLOWMETER CALIBRATION

In order to find the linear calibration coefficient, C in (2), a reference flowmeter with a calibration certificate developed with standards tracable to NIST and in accordance with ANSI Z540-1-1994 was used in-line to perform a master meter calibration. This calibration was performed using high purity, reactor grade sodium from MSSA (France) in the sodium loop described in [24], [25]. The calibration coefficient was solved for in (11).

$$C = \frac{Q_{REF}}{Q_{IUT}} = Q_{REF}\frac{4BK_BK_WK_E}{\pi V_m d} \tag{11}$$

This article has been accepted for publication in a future issue of this journal, but has not been fully edited. Content may change prior to final publication. Citation information: DOI 10.1109/JSEN.2021.3079713, IEEE Sensors Journal

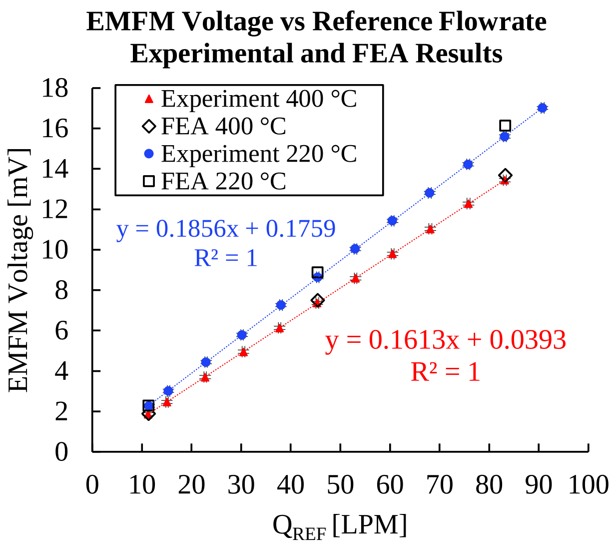

Fig. 7. Experimental and FEA induced voltage as a function of sodium flowrate at 400 and 220°C. FEA results deviate <3.2% from experimental trendline. Error bars have been provided for EMFM voltage and reference flow rate, representing type A and B uncertainty in the 90 measurements taken for each flow rate and temperature

Where Q_{REF} is the reference flow rate in m^3/s. The reference flow meter used for calibration was a Foxboro M83, 1" vortex shedder type meter (model: 83F-T01S2STRJA-G). The flow meter possessed a minimum startup flow rate of 7.6 LPM (2 GPM) and a maximum flow rate of 189 LPM (50 GPM). The maximum operating temperature of the flow meter was listed as 420 °C and it possessed an accuracy of $\pm$0.5% of reading over the entire working range of the meter.

A procedure for the master meter method calibration of the EM flowmeter is described below:

1) Install the reference flowmeter (REF) and EM flowmeter instrument under test (IUT) in series along the calibration loop, ensuring that the appropriate inlet and exit flow development length are achieved as listed for both flow meters. For the ANL EMFM a length of 10 pipe diameters upstream and 3 pipe diameters downstream from the flowmeter is sufficient [9].
2) If the inner wall of the electromagnetic flow meter has not been sufficiently wetted with sodium, the operator shall establish an environment to wet the flowmeter before calibration. The sodium temperature shall be raised to 400°C and the flow rate shall be set to 22.4 LPM. Under isothermal, constant flow conditions, a wetted condition may be determined when the measured voltage of the flowmeter is steady for a period of at least 2 hours.
3) Bring system to desired calibration temperature, below the maximum working temperature of the reference flowmeter (420°C) and the EM flowmeter (550°C).
4) Ensure the entire system is isothermal, ($\approx \pm 2°C$), especially in the region where the two flowmeters are installed, to avoid uncertainty in process fluid density.
5) Ensure that the performance of the reference flow meter reflects the listed accuracy to ensure proper functionality by taking 90 measurements at 1 Hz at a flow rate near the middle of the calibration range (45.4 LPM in this case) and calculating the standard deviation of the mean of those measurements. This will also ensure the system is able to achieve equilibrium.
6) Set the system to a desired flow rate within the calibrated range of the reference flow meter (7.6-189 LPM), and begin acquiring data from the flow meters when the temperature and flow rates are at steady state. In order to achieve statistical significance, 90 measurements shall be attained for each calibration condition at an acquisition rate of 1 Hz.
7) Repeat step 6 for each flow rate and temperature of interest for calibration.
8) The calibration coefficient, C, may be calculated using (11) for each flow rate and temperature tested.

A photograph of the ANL EMFM installed in series with the reference flowmeter can be found in Fig. 8.

Fig. 9 presents the flowrate of the reference flowmeter, measured voltage of the ANL EMFM and sodium temperature as a function of time during the wetting phase of the calibration (step 2 of procedure). As can be seen the measured voltage of the EMFM remains constant for a period of >2 hrs, ensuring the tube has been fully wetted and the electrical contact resistance between the sodium and inner wall of the flowtube has been minimized. Once the stainless tube wall has been wetted the sodium-wall interface will have a contact resistance of approximately 0.006 $\mu\Omega/cm^2$ so will have a negligible effect on the measurement accuracy or response time [26].

Calibration data was taken according to step 6 of the procedure at sodium temperatures of 400 °C and 220 °C. Calibration was performed at nominal flowrates of 11.4 LPM (3 GPM), and 15.1-83.3 LPM (4-22 GPM) in increments of 7.6 LPM (2 GPM). Data was also taken at 90.9 LPM (24 GPM) for sodium at 220 °C. Fig. 10 provides the uncalibrated ANL EMFM data, generated using (2), plotted as a function of reference flow rate. As can be seen, both the instrument under test and reference flow meter possess good precision with tight error bars for the 90 measurements at 1 Hz. The error is also calculated for the instrument under test, with respect to the reference flow meter. Errors as large as 9.5% for the uncalibrated flowmeter reveal the importance of calibration. Recall the FEA analysis yielded an error less than 3.2% for the same flow range. Thus, if a calibration is not possible, an FEA model should be utilized to determine flowrates as opposed to the K factors of Eqs. 2-5.

The calibration coefficient was calculated using (11) for all calibration set points and temperatures. Fig. 11 presents the calibration coefficients as a function of flow rate and induced voltage. The enhanced deviation of the calibration coefficient from unity at high flow rates is likely due to a distortion of the magnetic field, as observed by [27] and [28] for short meters with high values of $\mu_0\sigma_e vd$. This distortion is a result of circulating electric end currents that create a diminished magnetic field at the entry and an enhanced magnetic field at the exit of the meter; thus the ultimate magnetic field distortion resembles the magnetic field being dragged along the axis of the flow tube. At high flow rates the induced voltage will be affected as the magnetic field in the region where the sensor leads are welded on will begin to diminish as a result of this effect. This can be accounted for by utilizing a power function fit to the calibration coefficient vs induced voltage to determine C in real-time, (12). It should be noted that the FEA was shown to account for this magnetic field distortion with good correlation to experimental data in Fig. 7.

$$C = 1.1899(V_m)^{0.0193} \tag{12}$$

VI. Uncertainty Analysis

The uncertainty analysis presented below is derived from the methods prescribed by the ISO Guide to Expression of Uncertainty in Measurement (ISO 1995a). [30]

Uncertainty for the calibration coefficient was calculated by propagating the sensitivity of C to the uncertainties associated with the constitutive variables in (11), known as type B uncertainties, as well as the uncertainty attributed to random fluctuations that occur during measurement, accounted for using (13), known as type A uncertainties.

$$U_{C,\sigma} = \frac{\sigma}{\sqrt{N}} = \sqrt{\frac{1}{N(N-1)}\sum_{i=1}^{N}(C_i - \bar{C})^2} \tag{13}$$

The following sensitivities, θ_i, are considered for error propagation to calculate the type B contribution to the overall calibration uncertainty:

$$\frac{\partial C}{\partial T_m}, \frac{\partial C}{\partial T_s}, \frac{\partial C}{\partial B}, \frac{\partial C}{\partial L}, \frac{\partial C}{\partial d}, \frac{\partial C}{\partial D}, \frac{\partial C}{\partial V_m}, \frac{\partial C}{\partial Q_{REF}}$$

The precision index and the bias limit can be calculated using the sensitivities and uncertainty budget values as:

$$S_R = \sqrt{\sum_{i=1}^{J_s}(\theta_i \frac{U_{s,i}}{\sqrt{N}})^2 + U_{C,\sigma}^2} \tag{14}$$

$$B_R = \sqrt{\sum_{i=1}^{J_b}(\theta_i U_{b,i})^2} \tag{15}$$

Where J_s and J_b are the total number of precision and bias uncertainties, θ_i is a particular sensitivity coefficient, and Us_i and Ub_i are the particular precision and bias uncertainties.

Finally, the total uncertainty can be calculated using the general law of uncertainty combination [31]:

$$U = \sqrt{B_R^2 + t_{\alpha,\nu_R} S_R^2} \tag{16}$$

Where t_{α,ν_R} is the t distribution for the confidence interval and degrees of freedom reported; in this case t_{α,ν_R}=2.0 for a 95% confidence interval.

The uncertainties were found for each calibration condition. For reference, Table II provides the uncertainty budget for a flowmeter calibration at 400°C, 22.7 LPM (6 GPM).

In order to determine the relative effect of each variable's contribution to the total uncertainty, Table III provides the sensitivity-uncertainty multiple for each variable. Note that the sensitivities for each variable were found numerically using Wolfram Mathematica v12.0 software.

TABLE II
Uncertainty Budget

Variable	Source	$U_{C,\sigma}$,$U_{s,i}$	$U_{b,i}$
C	$U_{C,\sigma}$	6.02E-04	-
T_m,T_s	Thermocouple	-	±3.0 °C
	NI 9213	-	±1 °C
Q_{REF}	Calibr. Cert.	±0.5%	-
	NI 9219	±0.3%	±4.5 mV
B	Gaussmeter	-	±0.1 mT
V_m	NI 9219	±0.1%	±0.08 mV
	Lead Position	-	±0.2%
L, d, D	Calipers	-	±0.025 mm

Flowmeter at ≈400°C, 22.7 LPM (6 GPM). The thermocouples are Omega type K, ungrounded 3.2 diameter probes. NI 9213 and 9219 are National Instruments data acquisition modules connected to a National Instruments cRIO 9024 chassis. The Gaussmeter is an F.W. Bell model 5180. The calipers are Mitutoyo model 500-474.

TABLE III
Sensitivity of Calibration

Variable	$U_{C,\sigma}$, $\theta_i \frac{U_{s,i}}{\sqrt{N}}$ ($\times 10^4$)	$\theta_i U_{b,i}$ ($\times 10^4$)
C	6.02	-
T_s	-	-1.25
T_m	-	-30.0
Q_{REF}	13.0	103
B	-	4.27
V_m	-1.14	-175
L	-	0.31
d	-	-3.87
D	-	-1.41

Flowmeter at ≈400°C, 22.7 LPM (6 GPM).

As can be seen, the bias error from the EM flowmeter voltage and the reference flowmeter measurement have the largest effect on the calibration uncertainty. The magnet temperature bias error also contributes significantly to the uncertainty; therefore it is important to position the magnet thermocouple in close proximity to the magnet to acquire accurate temperature readings to calculate K_B, (3).

The uncertainty in the calibration coefficient, as derived above, has been plotted as a function of reference flow rate for temperatures of 220 and 400°C, Fig. 12. When performing the master meter method of calibration in conformance with ANSI/NCSLZ540.3, the reference meter should be 4 times as precise as the instrument under test, typically referred to as the test uncertainty ratio (TUR). The reference meter possesses an uncertainty of ±0.5%, Table II. Thus the minimum uncertainty of the instrument under test is $4 \cdot 0.5\% = 2.0\%$. This has been included as a dotted line in Fig. 12 and represents the minimum reportable uncertainty for the flowmeter calibration.

VII. Conclusions

A permanent magnet flowmeter capable of withstanding submersion in radioactive sodium at 550 °C was designed, constructed and analyzed.

A finite element analysis was performed to assess the predicted induced voltage as a function of flow rate and temperature, and used to determine the relative permeability of the yoke material as well as the sensitivity of the sensor lead

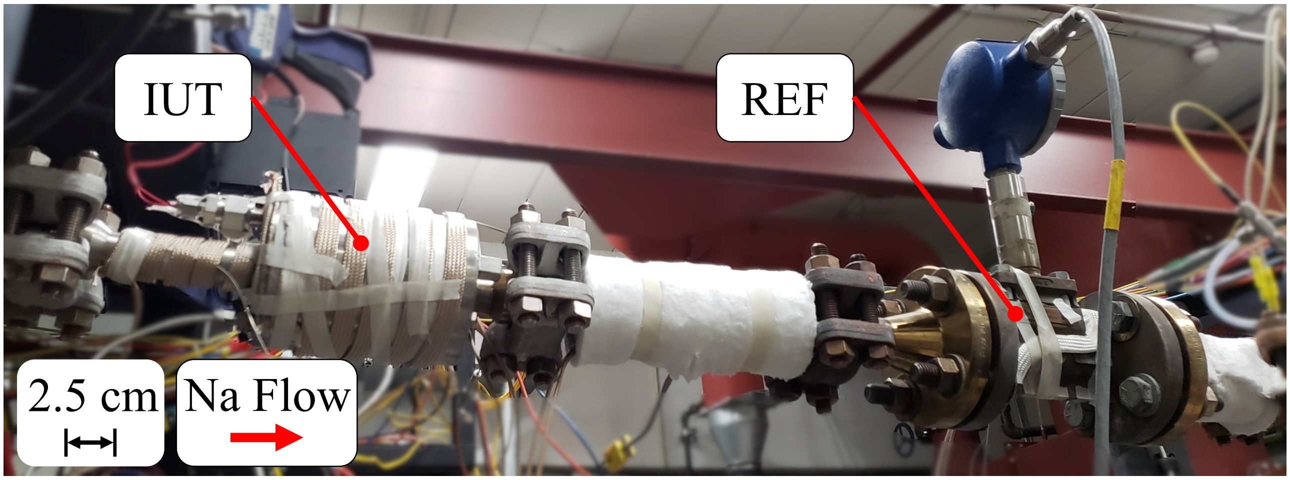

Fig. 8. Photo showing the Instrument Under Test (IUT) and the Reference (REF) flowmeter installed in the University of Wisconsin-Madison liquid sodium calibration loop. The loop possesses a moving magnet pump that is controlled by a variable frequency drive [29].

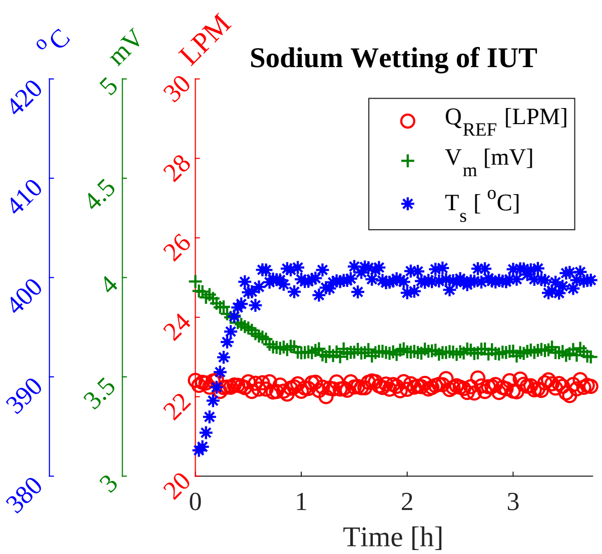

Fig. 9. Wetting of IUT at 400°C and 22.4 LPM. As can be seen, there was no change in V_m for a period of $>$2.5 hrs.

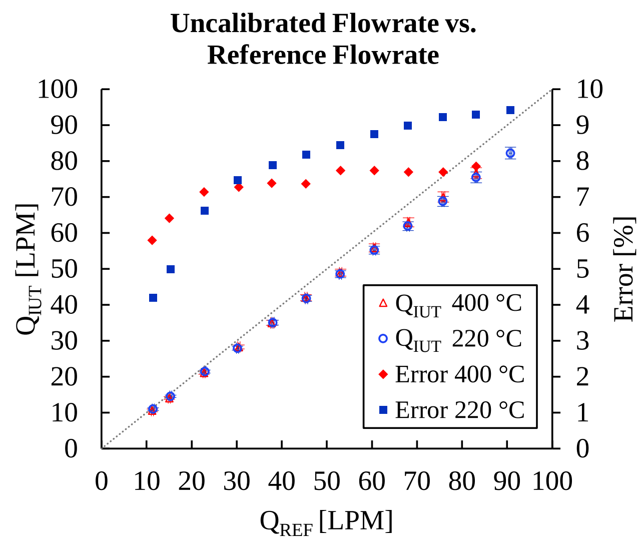

Fig. 10. Uncalibrated flow rate of instrument under test (EM flowmeter) as a function of the reference flow meter (vortex shedder) from 11.4-90.8 LPM (3-24 GPM) at sodium/magnet temperatures of 220°C and 400°C. Error of the instrument under test with respect to the reference also provided

geometric tolerance. The FEA model may be utilized in lieu of semi-empirical (2) to create a digital twin of the flowmeter to determine flowrate from voltage and temperature readings-eliminating the need to perform an expensive calibration for flow measurement applications where uncertainty quantification is less critical.

A calibration procedure was detailed for the flow meter, accounting for unique phenomena such as surface wetting, to acquire statistically significant data. An uncertainty analysis was performed to assess the accuracy of the calibration coefficient at sodium temperatures of 220 and 400 °C, with flow rates ranging from 11.4-90.9 LPM. An uncertainty on the order of 2-3.6% was reported for the flowmeter calibration.

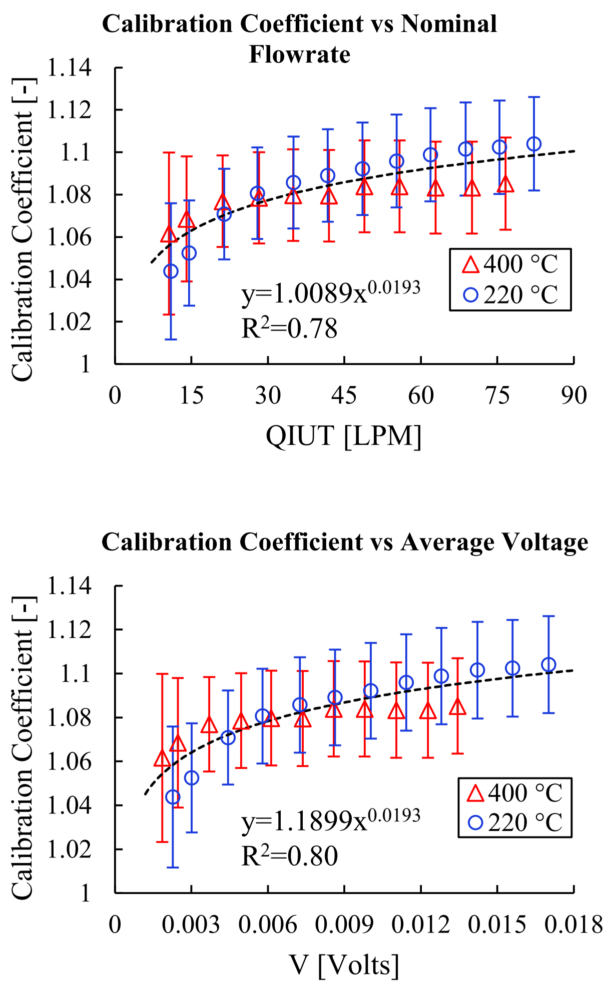

Fig. 11. Calibration coefficient calculated for data in Fig. 10 using (11). A power function was fit to the data. The calibration coefficient variation may be due to distortion in the magnetic field due to the conductive sodium dragging it along as it flows through the flow meter.

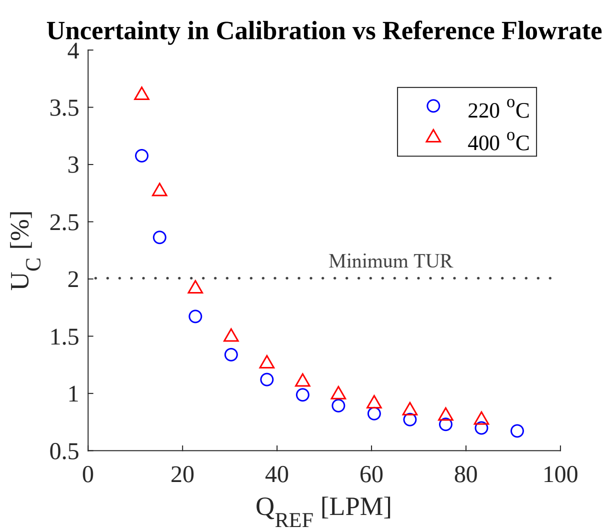

Fig. 12. Uncertainty in calibration coefficient as a function of the reference flowmeter for sodium at 220 and 400°C

ACKNOWLEDGMENT

Thank you to Alice Caponiti, Tom Sowinski, and Brian Robinson at the US Department of Energy and Robert Hill at Argonne National Laboratory for their continued support.

Thank you to William Toter and Robin Reierson for their sound engineering advice and welding craftsmanship. Thank you to Paul Brooks, James Schneider, Andrew Napora, and Dr. Jordan Rein at UW-Madison for flowmeter calibration assistance. Finally, thank you to Dr. Heeju Choi, Dr. Melania Jasinski, and Bryce Wall for providing and permitting the publication of the magnetic properties of EEC 18-T550.

REFERENCES

[1] G. E. Turner, "Liquid Metal Flow Measurement (Sodium) State-of-the-Art Study," Liquid Metal Engineering Center, Tech. Rep., 1968.

[2] O. Foust, *Sodium-NaK Engineering Handbook Volume III*. New York: Gordon and Breach, 1978.

[3] E. Furlani, *Permanent Magnet and Electromechanical Devices*. San Diego: Academic Press, 2001.

[4] A. Palasyuk, E. Blomberg, R. Prozorov, L. Yue, M. J. Kramer, R. W. McCallum, I. E. Anderson, and S. Constantinides, "Advances in characterization of non-rare-earth permanent magnets: Exploring commercial alnico grades 5-7 and 9," *Jom*, vol. 65, no. 7, pp. 862–869, 2013.

[5] J. Liu, P. Vora, P. Dent, and M. Walmer, "Thermal Stability and Radiation Resistance of SmCo Based Permanent Magnets," in *Proceedings of Space Nuclear Conference 2007*, Boston, 2007.

[6] Weathered, Kultgen, Kent, Grandy, Sumner, Moisseytsev, and Kim, "Thermal Hydraulic Experimental Test Article – Status Report FY2020," Argonne National Laboratory, Lemont, Tech. Rep., 2020.

[7] Kultgen, Weathered, Kent, and Grandy, "Mechanisms Engineering Test Loop (METL) Operations and Testing Report FY2020," Argonne National Laboratory, Lemont, Tech. Rep., 2020.

[8] J. Shercliff, *The Theory of Electromagnetic Flow-Measurement*. Cambridge University Press, 1962.

[9] W. Gray and E. Astley, "Liquid Metal Magnetic Flowmeters," *Journal of Instrument Society of America*, 1954.

[10] M. Hvasta, "Designing & Optimizing a Moving Magnet Pump for Liquid Sodium Systems," Ph.D. dissertation, University of Wisconsin-Madison, Madison, 2013.

[11] J. K. Fink and L. Leibowitz, "Thermodynamic and Transport Properties of Sodium Liquid and Vapor," pp. 1–238, 1995. [Online]. Available: http://www.osti.gov/servlets/purl/94649-gXNdLI/webviewable/

[12] C. Ho and T. Chu, "Electrical Resistivity and Thermal Conductivity of Nine Selected AISI Stainless Steels," American Iron and Steel Institute, Washington D.C., Tech. Rep., 1977.

[13] H. Choi and B. Wall, "Personal Correspondence with EEC," 2020.

[14] O. Foust, *Sodium-NaK Engineering Handbook Volume V*, O. Foust, Ed. New York: Gordon and Breach, 1979.

[15] G. Vijayakumar, B. K. Nashine, K. K. Rajan, and P. Kalyanasundaram, "Development and testing of PM flowmeter with Samarium Cobalt magnet assembly," *Energy Procedia*, vol. 7, no. December, pp. 630–637, 2011.

[16] C. H. Chen, M. Huang, A. Higgins, D. Lee, and S. Liu, "Improved Mechanical Properties and Thermal Stability of Sm-Co High Temperature Magnets Resulting From Surface Modifications," *Journal of Iron and Steel Research International*, vol. 13, no. SUPPL. 1, pp. 112–118, 2006. [Online]. Available: http://dx.doi.org/10.1016/S1006-706X(08)60168-5

[17] J. Hartmann and F. Lazarus, "Experimental investigations of the flow of mercury in a homogeneous magnetic field," *Mathematisk-fysiske Meddelelser*, vol. 15, no. 7, pp. 1–45, 1937. [Online]. Available: http://gymarkiv.sdu.dk/MFM/kdvs/mfm 10-19/mfm-15-7.pdf

[18] K. Messadek and R. Moreau, "On the measurement of the Hartmann layer thickness in a high magnetic field," *Physics of Fluids*, vol. 16, no. 9, pp. 3243–3246, 2004.

[19] R. J. Lingwood and T. Alboussière, "On the stability of the Hartmann layer," *Physics of Fluids*, vol. 11, no. 8, pp. 2058–2068, 1999.

[20] *COMSOL Multiphysics CFD Module User 's Guide*, 2016. [Online]. Available: https://doc.comsol.com/5.3/doc/com.comsol.help.cfd/CFDModuleUsersGuide.pdf

[21] "Magnetic Permability: Why Are Some Materials Attracted By A Magnet And Others Are Not?" pp. 1–5. [Online]. Available: https://www.duramag.com/techtalk/tech-briefs/magnetic-permeability-why-are-some-materials-attracted-by-a-magnet-and-others-are-not/

[22] N. Wilson and P. Bunch, "Magnetic permeability of stainless steel for use in acclerator beam transport systems," *Conference Record of 1991 IEEE Particle Accelerator Conference*, pp. 2322–2324, 1991.

[23] R. Bowers, "Magnetic Susceptibility of Sodium Metal," *Physical Review*, vol. 100, no. 4, 1955.

[24] M. Weathered, J. Rein, M. Anderson, P. Brooks, and B. Coddington, "Characterization of Thermal Striping in Liquid Sodium With Optical Fiber Sensors," *Journal of Nuclear Engineering and Radiation Science*, vol. 3, no. October, 2017.

[25] M. T. Weathered, "Characterization of Sodium Thermal Hydraulics with Optical Fiber Temperature Sensors," Ph.D. dissertation, University of Wisconsin-Madison, 2017.

[26] Vandenberg, "Electrical Contact Resistance Between Sodium and Stainless Steel," Knolls Atomic Power Laboratory, Tech. Rep., 1956.

[27] D. Pfister, "D-C Magnetic Flowmeter for Liquid Sodium Loops," *Nucleonics*, vol. 15, no. 10, 1957.

[28] T. Shimizu and N. Takeshima, "A numerical study on faraday-type electromagnetic flowmeter in liquid metal system, (II) analysis of end effect due to saddle-shaped small-sized magnets with FALCON code," *Journal of Nuclear Science and Technology*, vol. 38, no. 1, pp. 19–29, 2001.

[29] M. G. Hvasta, W. K. Nollet, and M. H. Anderson, "Designing moving magnet pumps for high-temperature, liquid-metal systems," *Nuclear Engineering and Design*, vol. 327, no. January, pp. 228–237, 2018. [Online]. Available: https://doi.org/10.1016/j.nucengdes.2017.11.004

[30] E. Mathioulakis and V. Belessiotis, "Uncertainty and traceability in calibration by comparison," *Measurement Science and Technology*, vol. 11, no. 6, pp. 771–775, 2000.

[31] C. Dietrich, *Uncertainty, Calibration and Probability*, 1st ed. CRC Press, 1991.